 doi:10.20944/preprints202103.0226.v1

Article

Digital Image Processing and Development of Machine Learning Models for the Discrimination of Corneal Pathology: An Experimental Model

Andres Bustamante-Arias[1], Abbas Cheddad[2] , Julio Cesar Jimenez-Perez[1] and Alejandro Rodriguez-Garcia[1,*]

[1] Tecnologico de Monterrey, School of Medicine & Health Sciences, Institute of Ophthalmology & Visual Sciences, Monterrey, 66278, Mexico
[2] Department of Computer Science and Engineering, Blekinge Institute of Technology, Karlskrona, SE-371 79, Sweden
* Correspondence: immuneye@gmail.com; Institute of Ophthalmology & Visual Sciences, School of Medicine & Health Sciences, Tecnologico de Monterrey, Monterrey, Mexico. Hospital Zambrano Hellion Av. Batallon de San Patricio 112 Real de San Agustin San Pedro Garza Garcia, Nuevo Leon, 66278, Mexico

Abstract: Machine learning (ML) has a large capacity to learn and analyze a large volume of data. This study aimed to train different algorithms to discriminate between healthy and pathologic corneal images by evaluating digitally processed spectral-domain optical coherence tomography (SD-OCT) corneal images. A set of 22 SD-OCT images belonging to a random set of corneal pathologies was compared to 71 healthy corneas (control group). A binary classification method was applied; three approaches of ML were used. Once all images were analyzed, representative areas from every digital image were also processed and analyzed for a statistical feature comparison between healthy and pathologic corneas. The best performance was obtained from transfer learning - support vector machine (TL-SVM) (AUROC = 0.94, SPE 88%, SEN 100%) and transfer learning – random forest (TL-RF) method (AUROC = 0.92, SPE 84%, SEN 100%), followed by convolutional neural network (CNN) (AUROC = 0.84, SPE 77%, SEN 91%) and random forest (AUROC = 0.77, SPE 60%, SEN 95%). The highest diagnostic accuracy in classifying corneal images was achieved with the TL-SVM and the TL-RF models. In image classification, CNN was a strong predictor. This pilot experimental study developed a systematic mechanized system to discern pathologic from healthy corneas.

Keywords: Artificial intelligence; machine learning; cornea; SD-OCT; keratoconus; ectasia; keratitis; random forest, convolutional neural network; transfer learning.

1. Introduction

Despite recent advances in corneal digital imaging analysis, an objective and reproducible system for preclinical detection and measurement of corneal pathologic changes is still an unmet goal. Standardized quantitative measurement of different corneal structural alterations, such as stromal thinning and edema, inflammatory infiltration, fibrosis, and scarring, are crucial for early detection, objective documentation, grading, and disease progression.

A major disadvantage of spectral-domain optical coherence tomography (SD-OCT) corneal pathology imaging is that it fails to provide precise measurement values associated with specific diseases compared to other technologies such as corneal topography-tomography and aberrometry that could guide clinicians to a more objective diagnostic analysis.

During the last two decades, computer science research has evolved like no other field in humankind. Artificial intelligence (AI) has an immense capacity to learn and analyze a large volume of data and, simultaneously, autocorrect and continues learning to improve the sensitivity and specificity as a diagnostic and disease progression tool in medicine. Hence, AI has a promising future application in ophthalmology. Recently,

 doi:10.20944/preprints202103.0226.v1

supervised ML has been applied to systematic identification and diagnosis of different ocular pathologies, including diabetic retinopathy[1,2], age-related macular degeneration[3–6], glaucoma[7–9], keratoconus[10–13], among others. Different deep learning and conventional machine learning methods of analysis have been used in ophthalmology; among the most commonly used ones are random forest (RF)[14], support vector machine (SVM)[15,16], convolutional neural network (CNN)[17,18], and transfer learning (TL)[19–21]. RF solves classification and regression problems based on rules to binary split data by assembling many decision trees for classification. In this model, the prediction is made by majority voting[22]. In SVM, a given labeled training data is submitted to an algorithm that outputs an optimal hyperplane which separates the elements of different groups[23]. CNN employs algorithms that use a cascade of multilayered artificial neural networks for feature extraction and transformation of data, and TL is a machine learning method where a model developed (eg., fine-tuned weights) for a task is reused as the starting point for a model on a second task[24]. These deep learning algorithms provide an extraordinary amount of information, which is crucial for data analysis, but also such information can be overwhelming and may significantly affect decision making.

This study aimed to train different AI algorithms to discriminate between healthy and pathologic corneal images by evaluating digitally processed SD-OCT corneal images.

2. Materials and Methods

A prospective, cross-sectional, pilot exploratory cohort study was designed. All patients read and signed informed consent to voluntarily participate in the study, which was previously approved by the Ethics and Research Committees of our institution (protocol registration No. CONBIOETICA-14-CEI-0003-2019 and 18-CI-14-120058, respectively), and conducted according to the tenets of the Declaration of Helsinki.

SD-OCT is now a conventional imaging diagnostic tool in the clinical environment that helps study the microstructural changes of different eye pathologies, including the cornea. SD-OCT provides non-contact in-vivo corneal cross-sectional, high-resolution images. The RTVue-100 (Optovue®, Fremont, CA. USA) SD-OCT corneal module permits a high-speed acquisition of image frames (1,024 axial scans in 0.4 seconds) with little motion artifacts, reducing background noise. This SD-OCT works at a wavelength of 830nm, and a speed of 26,000 A-scans per second[25].

The experiments shown below were performed on a dataset comprising corneal images belonging to a random set of corneal pathologies. This set of images was compared to healthy corneas (control group). The problem was confronted using binary classification methods. The quest illustrates three approaches:

1. Traditional machine learning, including RF and SVM.
2. Deep learning using end-to-end CNN.
3. TL using the pre-trained model (e.g., AlexNet)[26].

A) Segmentation and Feature Extraction

Cornea Scan Postprocessing: Digital SD-OCT images usually are contaminated with noise inherited from the sensor (Figure 1a). This problem is easily circumvented by applying a 2D median filter. Nevertheless, in order to extract statistical features from these images, one must do what is known in the imaging domain as image segmentation, which partitions the image into different segments (a.k.a., regions), which are, in our case, three segments (background, corneal image, and region of interest) as shown in Figure 1. In the figure, the cornea region mask is obtained by applying contrast limited adaptive histogram equalization (CLAHE) followed by fixed thresholding (Figure 1b). The background region is simply the inverse of the mask (Figure 1c). The region of interest (ROI) is obtained using our fast image segmentation method based on Delaunay Triangulations,[27,28] which is fully automatic and does not require specifying the number of clusters, as is the case with the k-means clustering[29] or the multilevel image thresholds using Otsu's method[30] (Figure 1d).

Preprints (www.preprints.org) | NOT PEER-REVIEWED | Posted: 8 March 2021 doi:10.20944/preprints202103.0226.v1

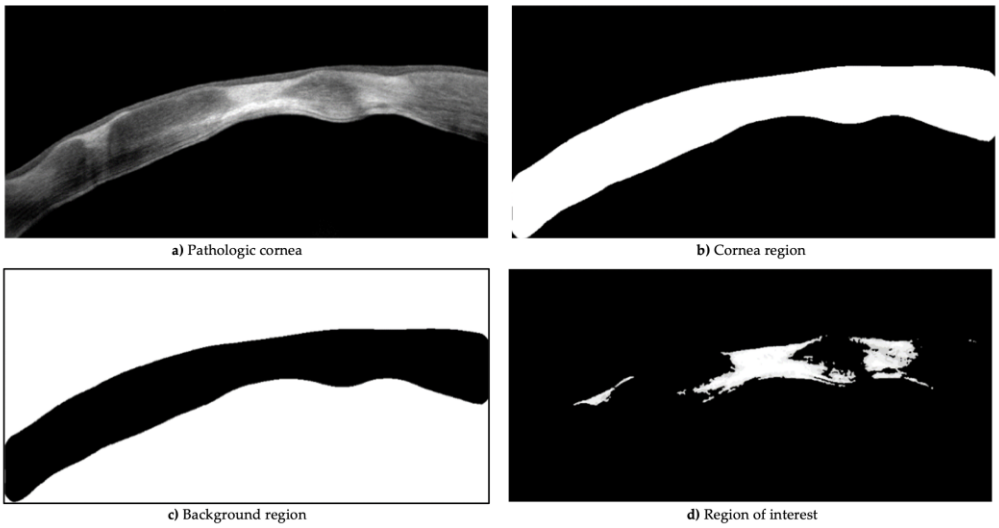

Figure 1. Digital image segmentation process. In order to extract statistical features, image segmentation was performed into different portions.

Feature Extraction: In image processing and its intersection with machine learning, feature extraction plays a crucial role in pattern recognition. The process starts by calculating a set of measured data from images intended to be informative and non-redundant, facilitating subsequent machine learning tasks. There is a plethora of features one can extract from images; however, in this study, we resorted to measuring a few simple statistical features, which are: 1) the mean intensity value, 2) the standard deviation of values, 3) the ratio of features ("/" denotes the ratio of two columns, eg., H/J is the ratio of column H and column J), and 4) the absorbance (Table 1). Absorbance is a transform made to the image, calculated by using $\ln(\mathrm{A}/\overline{\mathrm{A}})$, where ln is the natural logarithm, A is the image, and $\overline{A}$ is the mean of the background region of A (Figure. 1).

Preprints (www.preprints.org) | NOT PEER-REVIEWED | Posted: 8 March 2021 doi:10.20944/preprints202103.0226.v1

Table 1. Sample of statistical features retrieved from all corneal SD-OCT digital images. Mean: mean intensity value; std: standard deviation value; "/": ratio of two columns; ROI: region of interest.

Column	B	C	D	E	F	G	H	I	J	K	L	M	N	O	P	Q	
Feature #	#1	#2	#3	#4	#5	#6	#7	#8	#9	#10	#11	#12	#13	#14	#15	#16	
Feature/ Patient	mean Cornea	meanCorneaAbsorbance	stdCornea	stdCorneaAbsorbance	B/D	C/E	meanROI	meanROIAbsorbance	stdROI	stdROIAbsorbance	H/J	I/K	H/B	J/D	I/C	K/E	Label
1	81.608 56298	1.632988 07	48.8462 7884	0.624292992	1.67072 2211	2.61573 9869	184.692 0656	2.569931007	30.5683 7893	0.16094087 4	6.04193 1959	15.9681 6861	2.26314 5666	0.62580 7731	1.57375 9818	0.25779 7021	Healthy
2	74.053 86141	1.164938 42	48.4912 1628	0.542022869	1.52716 0321	2.14924 2194	177.471 7582	2.023791252	29.5678 8087	0.16810316 7	6.00218 0507	12.0389 8352	2.39652 2677	0.60975 746	1.73725 1702	0.31014 0358	Healthy
3	90.311 20278	2.137742 167	57.1522 065	0.714624194	1.58018 7508	2.99142 1483	201.036 2925	3.146969188	14.6166 5438	0.07157747 3	13.7539 1983	43.9659 1629	2.22603 9365	0.25574 9608	1.47209 9506	0.10016 0999	Pathologic
4	69.848 67255	1.466197 69	42.5004 1774	0.607825603	1.64348 2023	2.41220 1266	157.582 0257	2.362927459	20.6386 2454	0.12815301 4	7.63529 6886	18.4383 2923	2.25604 8969	0.48560 9922	1.61160 2224	0.21083 8459	Healthy
5	107.03 24462	3.380685 912	51.7275 7053	0.620774315	2.06915 6643	5.44591 7832	206.947 3494	4.184606264	20.4003 243	0.09684122	10.1443 1665	43.2110 0296	1.93350 1072	0.39438 0097	1.23779 8001	0.15600 0688	Pathologic

B) Experimental Set-up

Random forest: The experimental set up to execute RF classification of data into healthy or pathologic images comprises two stages. The bag of decision trees is set to 50 growing trees (this number provides the right balance between AUC, processing time, and memory usage) in the training stage, which was used with a training set of 50 control and 15 pathologic images. The RF constructs decision trees based on the predictive characteristics of the features in Table 1. See also Figure 2 for a visualization of three out of the fifty trees. Figure 3 depicts how RF optimizes its performance across several growing trees (50 trees in our case) by performing out-of-bag (OBD) error calculation. The training phase converges into a model that we used, in the second stage, on a new validation test dataset comprising 21 controls and 7 pathologic images.

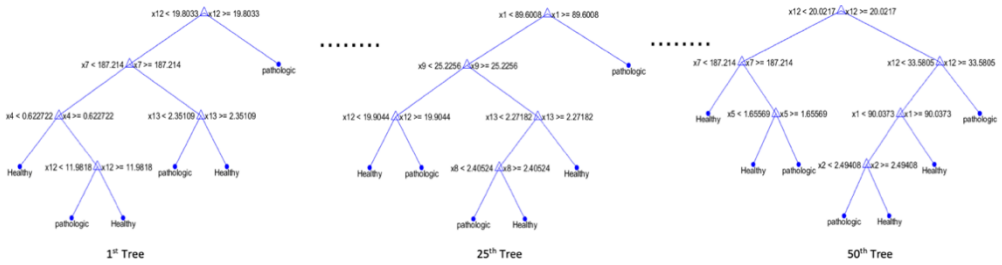

Figure 2. Random forest tree visualization. Ensemble classifiers from the aggregation of multiple decision trees.

Preprints (www.preprints.org) | NOT PEER-REVIEWED | Posted: 8 March 2021 doi:10.20944/preprints202103.0226.v1

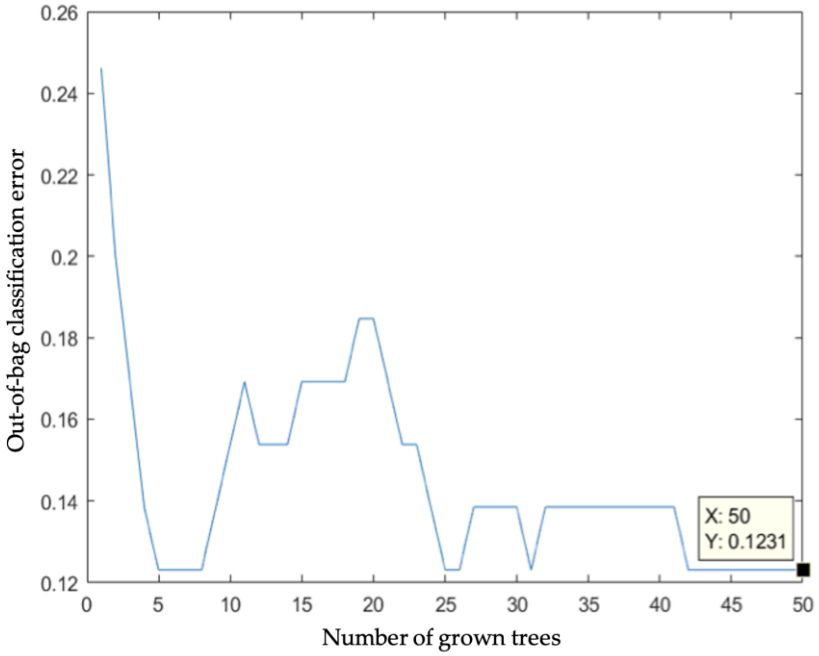

Figure 3. Random forest classification error minimization across the growing trees during training. RF optimizes its performance across several growing trees (50 trees) by performing out-of-bag (OBD) error calculation.

Convolutional Neural Network: CNN is a deep learning method and architecture that is well known in its capabilities for image classification. Input image dimensions are fixed to [227 227 3] (to match that of the AlexNet pre-trained model input size requirement), and the fully connected layer is set to two classes (healthy/pathologic). The architecture embodies three convolution layers, each of which has a filter size of 5-by-5, the activation function is set to the rectified linear unit (ReLU), and the number of epochs is set to eight. Images are fed directly to the CNN classifier with the same training and testing proportions as in section A.

Transfer Learning: In TL, the statistical model we use for prediction had been pre-trained on an enormous data set of natural images (eg., millions of samples); and the weights are then used in local learning. Features were augmented to yield 4096 features, which are then fed to classifiers with the same training and testing proportions as in section A. They used shallow learning classifiers are the SVM and RF.

Statistical metrics analysis: We categorized the registries in cases with corneal pathology and healthy corneal OCT entries. We used traditional machine learning, including random forest (RF) and support vector machine (SVM); deep learning using the convolutional neural network (CNN); and transfer learning (TL) using a pre-trained model (e.g., AlexNet). Then we applied the algorithm to another image matrix and finally measured the model precision, relative risk, sensitivity, specificity, negative predictive, and positive predictive values of the algorithm. Receiver operating characteristic (ROC) curves were analyzed to determine the optimal cut-off values, sensitivity, and specificity. The area under the curve (AUC) was used as a measure of accuracy. Accuracy was measured on the test dataset (correctly predicted class/total testing class) × 100. All measurements are reported as the average of 10 runs on a random selection of samples to eliminate any training/test dataset selection bias. For all models, the data was divided according to the same ratio shown in Table 2.

Preprints (www.preprints.org) | NOT PEER-REVIEWED | Posted: 8 March 2021 doi:10.20944/preprints202103.0226.v1

Table 2. Training and test data ratio.

	Healthy	Pathologic
Train data set	50 (77%)	15 (23%)
Test data set	21 (75%)	7 (25%)
Sum	71 (76%)	22 (24%)

All of the experiments, including the developed algorithms, were implemented using MATLAB ver. 9.5.0.944444 (R2018b) and IP Toolbox ver. 10.3 running on a 64-bit workstation with Windows 10 and 32.GB of RAM, 2.60 GHz.

3. Results

A total of 93 SD-OCT corneal images were registered in the study, 71 images formed part of the control group, and 22 pathologic images were included in the experimental group. The latter comprised 14 (63.6%) ectatic corneas and 8 (36.4%) corneas with infectious keratitis. The total analyzed corneas belonged to 55 (59.2%) women and 38 (40.8%) men. The mean age of patients in the experimental group was 38.68 ± 11.74 years, and in the control group, 45.56 ± 20.69 years.

We tested each model sequence's accuracy to assign the entry as pathologic or healthy. The RF method (AUROC = 0.77, SPE 60%, SEN 95%) had the lowest precision in the set (86.07%, ±5.44); however, the model only used 16 possible features extracted from the data, followed by CNN (AUROC = 0.84, SPE 77%, SEN 91%). Figure 4 displays the importance of statistical features of images analyzed by RF. The measure represents the increase in prediction error for any given variable if that variable's values are permuted across the out-of-bag observations. This measure is computed for every tree, then averaged over the entire ensemble, and divided by the standard deviation over the entire ensemble. It appears that features 12, 13, and 15 (e.g., corresponding to columns M, N, P in Table 1) are the most important in this classification model (Figure. 4).

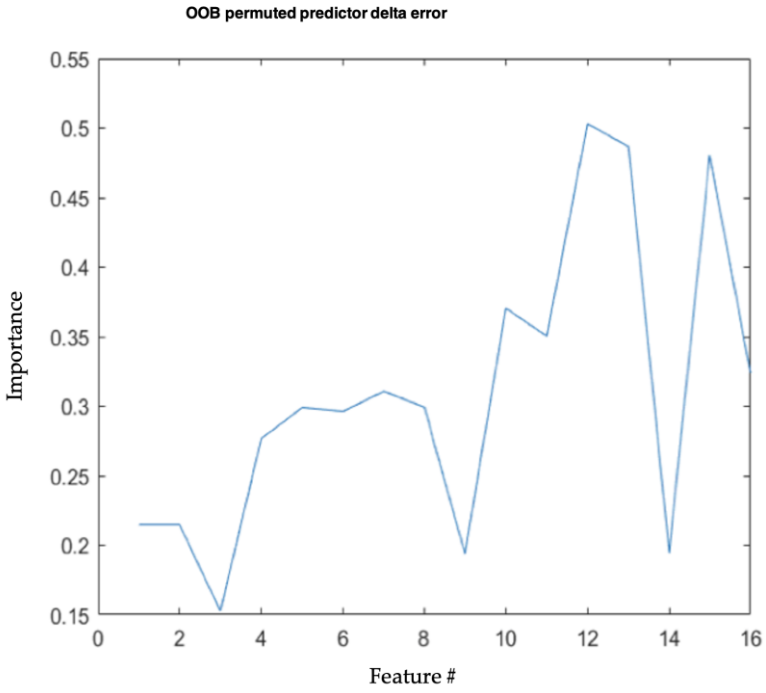

Preprints (www.preprints.org) | NOT PEER-REVIEWED | Posted: 8 March 2021 doi:10.20944/preprints202103.0226.v1

Figure 4. Features importance using the random forest method. Represents the increase in prediction error for any given variable if the values of that variable are permuted across the out-of-bag observations.

Algorithms that used more (4,096) had higher precision. The transfer learning-SVM model yielded the best results (TL-SVM. AUROC = 0.94, SPE 88.12%, SEN 100%) followed by the transfer learning-RF model (TL-RF. AUROC = 0.92, SPE 84%, SEN 100%). The visualization of this classification's performance can be further examined in Figure 5 showing the best performing test's confusion matrices from the 10 random tests for each algorithm. Table 3 summarizes the outcomes of the constructed models.

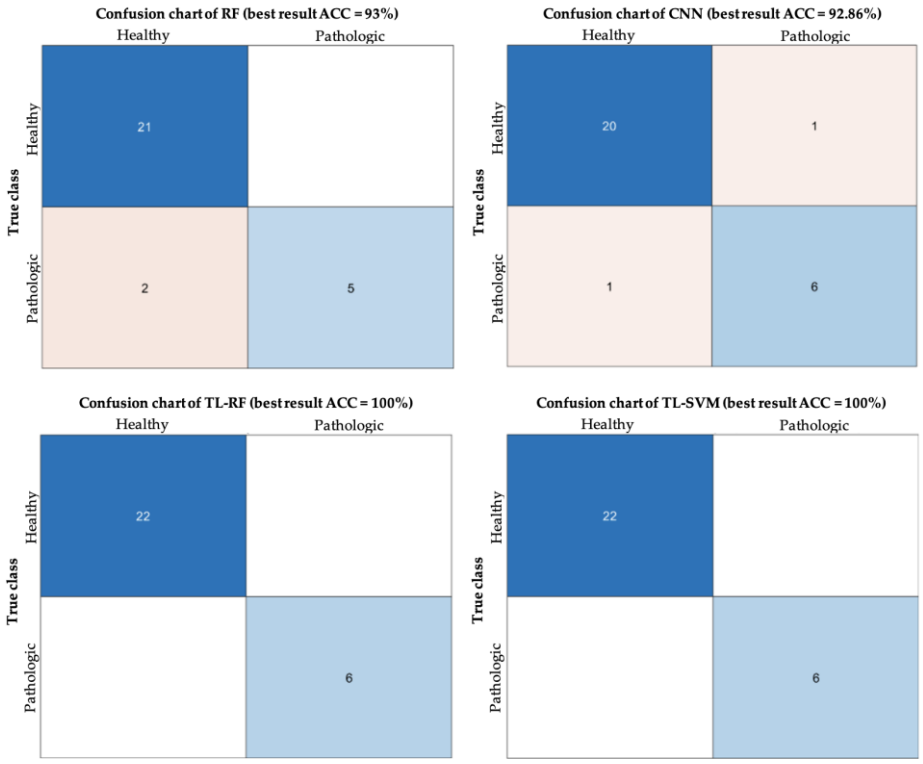

Figure 5. Confusion charts. Performance visualization using confusion matrix charts for the examined classification problem using the four different approaches (best accuracy out of the ten tests).

Table 3. Performance of the classification methods using different algorithms. (*) All metrics are the average over 10 runs (**) Area under the curve (-) CNN extracts its own features automatically from images. PPV: positive predictive value; NPV: negative predictive value.

Method	# of Features	Accuracy (%)	Specificity	Sensitivity (Recall)	PPV	NPV	Youden Index	AUC**
RF	16	86.07±5.44	0.60±0.20	0.95±0.05	0.88±0.05	0.83±0.16	0.55±0.19	0.77±0.10
CNN	-	86.79±6.95	0.77±0.16	0.91±0.04	0.92±0.06	0.71±0.13	0.67±0.19	0.84±0.10
TL-SVM	4,096	97.14±2.82	0.88±0.12	1.00	0.96±0.04	1.00	0.88±0.12	0.94±0.06
TL-RF	4,096	96.07±4.89	0.84±0.18	1.00	0.95±0.05	1.00	0.84±0.18	0.92±0.09

4. Discussion

AI is an upcoming technology in medicine that enables us to facilitate early detection; diagnosis accuracy; objective evaluation of disease progression; and detailed follow-up of therapeutic results of certain ophthalmologic disorders, particularly those most related to

 doi:10.20944/preprints202103.0226.v1

images of specific ocular structures, like the cornea, iris, lens, and retina.[24] It is a powerful tool that permits us to increase the diagnostic sensitivity and specificity of ophthalmic pathology[31].

The analysis of the corneal shape, refractive power, and in-depth microstructural changes related to degenerative, infectious, or inflammatory pathologies has significantly evolved in recent years through the development of topography, tomography, and aberrometry, which yield more accurate corneal measurements. Because these devices generate multiple maps and images of the cornea, the amount of data available from each acquisition may be overwhelming. Therefore, machine learning algorithms are being applied for early detection and accurate progression analysis of different corneal conditions, including keratoconus and endothelial health[12,31,32]. Currently, refractive surgery screening is the most fertile field for machine learning development in corneal disease. The reason for this is the increased risk of iatrogenic post-LASIK keratectasia due to unrecognized preoperative evaluation[12].

We tested different machine learning algorithms' performance for the discrimination between pathologic and healthy corneas to optimize their role in early detection, differentiation, and monitoring disease progression of different corneal pathologies. Artificial neural networks like CNN are strong predictors in image classification, with the advantage of dealing with noisy and missed clinical data, understanding complex data patterns in a way not possible for linear and non-linear calculations. However, this model requires massive clinical datasets (in the order of tens of thousands) for proper training[33], explaining why the CNN model performed poorly with the limited data set used for analysis in the present study[1]. Moreover, the availability of large training datasets is not always feasible, especially in corneal imaging analysis, where there are specific difficulties, including the devices´ high costs, technical acquisition challenges, and methodology differences that prevent building large datasets, thus making it a challenging task, if not impossible. When analyzing large datasets, there is a need for high computational power, limiting availability and increasing costs.

On the other hand, our results highlight the benefit of adopting the TL approach. A linear solution (two dimensional) is impossible in many ophthalmologic cases; therefore, getting a solution in a higher-dimensional dataset is required. An advantage of the TL-RF method is that it can model nonlinear class boundaries and may give variable importance, but at the same time, it may be slow, and it may be difficult to get insights into the decision rules. The TL-SVM solves the linearity problem with a relatively less computational cost using the kernel trick; a function used to obtain nonlinear variants of a selected algorithm[23]. In the present study, the highest diagnostic accuracy in classifying normal from pathologic corneal images was achieved with the TL-SVM and the TL-RF models in this order. Although transfer learning models (e.g., AlexNet) are models that have been trained to extract reliable and unique features from millions of raw images, it is proven here that their image descriptors can be extended to medical images.

Indeed, random forest learning models can achieve satisfactory outcomes with small datasets, but with the inconvenience of requiring a manual selection of specific visual features before classification. This condition can result in a set of suboptimal features that limits the application of the algorithms[31]. RF generates meta-models or ensembles of decision trees, and it is capable of fitting highly nonlinear data given relatively small samples[34]. RF reached this performance with merely 16 features (values), a strong indication that if more statistical features (hypothetically driven by ophthalmology experts) are added, the model may, with overwhelming probability, outperform CNN in this small dataset. Additionally, unlike other deep learning models, RF models are capable of pinpointing individual feature significance, which can help trace back diseases and trigger scientific discovery or physiological new findings.

Considering potential future research directions, we envision extending this work to classify different corneal disease sub-types; this will eventually aid clinicians in their diagnostic procedures. Furthermore, we aim to develop algorithms for risk prediction of corneal disease, which will help us identify individuals at higher risk of developing a

corneal disease (e.g., personalized medicine), hence improving its earlier detection before the disease reaches a devastating stage. However, as mentioned before, the necessity of collecting a substantial amount of data to get more accurate predictions and also to be able to use RF algorithms that are more suitable for image analysis is imperative, but an arduous task[35,36].

5. Conclusions

Applying AI optimal algorithms to different corneal pathologies for early detection, accurate diagnosis, and disease progression is a challenging job. There are economic limitations related to the high costs of equipment, technical acquisition challenges, and differences in the methodologic analysis that make it difficult to build large and reliable datasets. Furthermore, without the availability of vast datasets to feed data-hungry machine learning, the algorithms would be limited in their capability to give reliable results.

In the present experimental study with limited dataset samples, TL-SVM and TL-RF showed better sensitivity and specificity indices, and hence, they were more accurate to discriminate between healthy and pathologic corneas. On the contrary, the CNN algorithm showed less reliable results due to the limited samples. We believe that this revolutionary technology will mark the beginning of a new trend in image processing and corneal SD-OCT analysis, differing from current tendencies, where different anatomic characteristics like reflectivity, shadowing, thickness, among others, are subjectively analyzed.

Author Contributions: Conceptualization, A.B-A and A.R-.; design of the work, A.B-A, A.C and A.R-G; analysis, A.C; acquisition of data, A.B-A: interpretation of data, A.B-A, A.C, J.C.J-P and A.R-G; drafting the work, A.B-A, A.C, J.C.J-P and A.R-G; writing, A.B-A, A.C, J.C.J-P and A.R-G; revising, A.B-A, A.C, J.C.J-P and A.R-G. All authors have read and agreed to the published version of the manuscript.

Acknowledgments: Susana Imperial Sauceda for corneal SD-OCT analyses.

Funding: The Immuneye Foundation, Monterrey, Mexico.

Conflicts of Interest: The authors declare no conflict of interest.

References

1. Gulshan, V.; Peng, L.; Coram, M.; Stumpe, M.C.; Wu, D.; Narayanaswamy, A.; Venugopalan, S.; Widner, K.; Madams, T.; Cuadros, J.; et al. Development and validation of a deep learning algorithm for detection of diabetic retinopathy in retinal fundus photographs. *JAMA* **2016**, *316*, 2402–2410, doi:10.1001/jama.2016.17216.
2. Ting, D.S.W.; Cheung, C.Y.-L.; Lim, G.; Tan, G.S.W.; Quang, N.D.; Gan, A.; Hamzah, H.; Garcia-Franco, R.; San Yeo, I.Y.; Lee, S.Y.; et al. Development and validation of a deep learning system for diabetic retinopathy and related eye diseases using retinal images from multiethnic populations with diabetes. *JAMA* **2017**, *318*, 2211–2223, doi:10.1001/jama.2017.18152.
3. Lee, C.S.; Baughman, D.M.; Lee, A.Y. Deep learning is effective for the classification of OCT images of normal versus age-related macular degeneration. *Ophthalmol. Retin.* **2017**, *1*, 322–327, doi:10.1016/j.oret.2016.12.009.
4. Burlina, P.M.; Joshi, N.; Pekala, M.; Pacheco, K.D.; Freund, D.E.; Bressler, N.M. Automated grading of age-related macular degeneration from color fundus images using deep convolutional neural networks. *JAMA Ophthalmol.* **2017**, *135*, 1170–1176, doi:10.1001/jamaophthalmol.2017.3782.
5. Aslam, T.M.; Zaki, H.R.; Mahmood, S.; Ali, Z.C.; Ahmad, N.A.; Thorell, M.R.; Balaskas, K. Use of a neural net to model the impact of optical coherence tomography abnormalities on vision in age-related macular degeneration. *Am. J. Ophthalmol.* **2018**, *185*, 94–100, doi:10.1016/j.ajo.2017.10.015.
6. Grassmann, F.; Mengelkamp, J.; Brandl, C.; Harsch, S.; Zimmermann, M.E.; Linkohr, B.; Peters, A.; Heid, I.M.; Palm, C.; Weber, B.H.F. A deep learning algorithm for prediction of age-related eye disease study severity scale for age-related macular degeneration from color fundus photography. *Ophthalmology* **2018**, *125*, 1410–1420, doi:10.1016/j.ophtha.2018.02.037.
7. Raghavendra, U.; Fujita, H.; Bhandary, S. V; Gudigar, A.; Tan, J.H.; Acharya, U.R. Deep convolution neural network for

accurate diagnosis of glaucoma using digital fundus images. *Inf. Sci.* **2018**, *441*, 41–49, doi:10.1016/j.ins.2018.01.051.

8. Li, Z.; He, Y.; Keel, S.; Meng, W.; Chang, R.T.; He, M. Efficacy of a deep learning system for detecting glaucomatous optic neuropathy based on color fundus photographs. *Ophthalmology* **2018**, *125*, 1199–1206, doi:10.1016/j.ophtha.2018.01.023.
9. Yousefi, S.; Kiwaki, T.; Zheng, Y.; Sugiura, H.; Asaoka, R.; Murata, H.; Lemij, H.; Yamanishi, K. Detection of longitudinal visual field progression in glaucoma using machine learning. *Am. J. Ophthalmol.* **2018**, *193*, 71–79, doi:10.1016/j.ajo.2018.06.007.
10. Ambrósio, R.J.; Lopes, B.T.; Faria-Correia, F.; Salomão, M.Q.; Bühren, J.; Roberts, C.J.; Elsheikh, A.; Vinciguerra, R.; Vinciguerra, P. Integration of Scheimpflug-based corneal tomography and biomechanical assessments for enhancing ectasia detection. *J. Refract. Surg.* **2017**, *33*, 434–443, doi:10.3928/1081597X-20170426-02.
11. Ruiz Hidalgo, I.; Rodriguez, P.; Rozema, J.J.; Ní Dhubhghaill, S.; Zakaria, N.; Tassignon, M.-J.; Koppen, C. Evaluation of a machine-learning classifier for keratoconus detection based on Scheimpflug tomography. *Cornea* **2016**, *35*, 827–832, doi:10.1097/ICO.0000000000000834.
12. Lopes, B.T.; Ramos, I.C.; Salomão, M.Q.; Guerra, F.P.; Schallhorn, S.C.; Schallhorn, J.M.; Vinciguerra, R.; Vinciguerra, P.; Price, F.W.; Price, M.O.; et al. Enhanced tomographic assessment to detect corneal ectasia based on artificial intelligence. *Am. J. Ophthalmol.* **2018**, *195*, 223–232, doi:10.1016/j.ajo.2018.08.005.
13. Hwang, E.S.; Perez-Straziota, C.E.; Kim, S.W.; Santhiago, M.R.; Randleman, J.B. Distinguishing highly asymmetric keratoconus eyes using combined Scheimpflug and spectral-domain OCT analysis. *Ophthalmology* **2018**, *125*, 1862–1871, doi:10.1016/j.ophtha.2018.06.020.
14. Meinshausen, N. Quantile Regression forests. *J. Mach. Learn. Res.* **2006**, *7*, 983–999.
15. Chang, C.-C.; Lin, C.-J. LIBSVM: A library for support vector machines. *ACM Trans. Intell. Syst. Technol.* **2011**, *2*, doi:10.1145/1961189.1961199.
16. Cortes, C.; Vapnik, V. Support-vector networks. *Mach. Learn.* **1995**, *20*, 273–297, doi:10.1007/BF00994018.
17. LeCun, Y.; Bengio, Y.; Hinton, G. Deep learning. *Nature* **2015**, *521*, 436–444, doi:10.1038/nature14539.
18. LeCun, Y.; Haffner, P.; Bottou, L.; Bengio, Y. Object Recognition with gradient-based learning. In *Shape, Contour and Grouping in Computer Vision*; Forsyth, D. A., Mundy, J. L., Gesú, V., Cipolla, R., Eds.; Springer-Verlag Berlin Heidelberg, Germany: 1999; pp. 319–345.
19. Freund, Y.; Schapire, R. A decision-theoretic generalization of on-line learning and an application to boosting. *J. Comput. Syst. Sci.* **1997**, *55*, 119–139.
20. Ayodele, T.O. Types of machine learning algorithms. In *New Advances in Machine Learning*; Zhang, Y., Ed.; IntechOpen, London, England: Rijeka, 2010.
21. Lu, W.; Tong, Y.; Yu, Y.; Xing, Y.; Chen, C.; Shen, Y. Applications of artificial intelligence in ophthalmology: General overview. *J. Ophthalmol.* **2018**, *2018*, 1–15, doi:10.1155/2018/5278196.
22. Segal, M. R. Machine learning benchmarks and random forest regression. *UCSF: Center for Bioinformatics and Molecular Biostatistics*. California, USA. Retrieved from https://escholarship.org/uc/item/35x3v9t4 (2004).
23. Schölkopf, B.; Smola, A. Learning with kernels: Support vector machines, regularization, optimization, and beyond. In Proceedings of the Adaptive Computation and Machine Learning Series; MIT Press, Cambdrige, Mass. USA. 2002.
24. Ting, D.S.W.; Pasquale, L.R.; Peng, L.; Campbell, J.P.; Lee, A.Y.; Raman, R.; Tan, G.S.W.; Schmetterer, L.; Keane, P.A.; Wong, T.Y. Artificial intelligence and deep learning in ophthalmology. *Br. J. Ophthalmol.* **2019**, *103*, 167–175, doi:10.1136/bjophthalmol-2018-313173.
25. Huang, D.; Duker, J.S.; Fujimoto, J.G; Lumbroso, B.; Schuman, J.S.; Weinred, R.N. *Imaging the Eye from Front to Back with RTVue Fourier-Domain Optical Coherence Tomography*, 1st ed.; Huang, D. Duker, J.S. Fujimoto, J.G Lumbroso, B. Eds.; Slack Incorporated, California, USA. 2010; ISBN 1556429630.
26. Krizhevsky, A.; Sutskever, I.; Hinton, G.E. ImageNet classification with deep convolutional neural networks. In *Advances in Neural Information Processing Systems 25*; Pereira, F., Burges, C.J.C., Bottou, L., Weinberger, K.Q., Eds.; Curran Associates, Inc., 2012; pp. 1097–1105.

27. Cheddad, A.; Condell, J.; Curran, K.; Kevitt, P.M. On points geometry for fast digital image segmentation in *The 8th International Conference on Information Technology and Telecommunication. Ireland: IEEE.* **2008**, 54–61.
28. Cheddad, A.; Mohamad, D.; Manaf, A.A. Exploiting voronoi diagram properties in face segmentation and feature extraction. *Pattern Recognit.* **2008**, *41*, 3842–3859, doi:10.1016/j.patcog.2008.06.007.
29. Lloyd, S. Least squares quantization in PCM. *IEEE Trans. Inf. Theory* **1982**, *28*, 129–137, doi:10.1109/TIT.1982.1056489.
30. Otsu, N. A Threshold selection method from gray-level histograms. *IEEE Trans. Syst. Man. Cybern.* **1979**, *9*, 62–66, doi:10.1109/TSMC.1979.4310076.
31. Lopes, B.T.; Eliasy, A.; Ambrosio, R. Artificial intelligence in corneal diagnosis: Where are we? *Curr. Ophthalmol. Rep.* **2019**, *7*, 204–211, doi:10.1007/s40135-019-00218-9.
32. Kolluru, C.; Benetz, B.; Joseph, N.; Lass, J.; Wilson, D.; Menegay, H. Machine learning for segmenting cells in corneal endothelium images. In Proceedings of the Medical Imaging 2019: Computer-Aided Diagnosis; Hahn, H.K., Mori, K., Eds.; SPIE, March 13 2019; p. 158.
33. Livingstone, D.J.; Manallack, D.T.; Tetko, I. V. Data modelling with neural networks: Advantages and limitations. *J. Comput. Aided. Mol. Des.* **1997**, *11*, 135–142, doi:10.1023/A:1008074223811.
34. Dasari, S.K.; Cheddad, A.; Andersson, P. Random forest surrogate models to support design space exploration in aerospace use-case. *In Artificial Intelligence Applications and Innovations. AIAI 2019. IFIP Advances in Information and Communication Technology*; MacIntyre, J., Maglogiannis, I., Iliadis, L., Pimenidis, E., Eds.; Springer: 2019; pp. 532–544.
35. Cheddad, A.; Czene, K.; Eriksson, M.; Li, J.; Easton, D.; Hall, P.; Humphreys, K. Area and volumetric density estimation in processed full-field digital mammograms for risk assessment of breast cancer. *PLoS One* **2014**, *9*, e110690, doi:10.1371/journal.pone.0110690.
36. Cheddad, A.; Czene, K.; Shepherd, J.A.; Li, J.; Hall, P.; Humphreys, K. Enhancement of mammographic density measures in breast cancer risk prediction. *Cancer Epidemiol. Biomarkers Prev.* **2014**, *23*, 1314–1323, doi:10.1158/1055-9965.EPI-13-1240.